5-2010

Digital Aperture Photometry Utilizing Growth Curves

William Chandler Overcast
woverca1@utk.edu

To the Graduate Council:

I am submitting herewith a thesis written by William Chandler Overcast entitled "Digital Aperture Photometry Utilizing Growth Curves." I have examined the final electronic copy of this thesis for form and content and recommend that it be accepted in partial fulfillment of the requirements for the degree of Master of Science, with a major in Physics.

Horace W. Crater, Major Professor

We have read this thesis and recommend its acceptance:

Wheeler K. McGregor, Christian G. Parigger

Accepted for the Council:
Carolyn R. Hodges

Vice Provost and Dean of the Graduate School

(Original signatures are on file with official student records.)

To the Graduate Council:

I am submitting herewith a thesis written by William Chandler Overcast entitled "Digital Aperture Photometry Utilizing Growth Curves." I have examined the final electronic copy of this thesis for form and content and recommend that it be accepted in partial fulfillment of the requirements for the degree of Master of Science, with a major in Physics.

Horace W. Crater, Major Professor

We have read this thesis
and recommend its acceptance:

Wheeler K. McGregor____

Christian G. Parigger_____

Acceptance for the Council:

Carolyn R. Hodges_____
Vice Provost and Dean of the
Graduate School

(Original signatures are on file with official student records.)

Digital Aperture Photometry Utilizing Growth Curves

A Thesis

Presented for the

Masters of Science

Degree

The University of Tennessee, Knoxville

William Chandler Overcast

May 2010

Acknowledgements

The author wishes to thank his major professor Dr. Horace W. Crater for his support and understanding throughout his time at UTSI. He would also like to extend his gratitude to the other members of his committee, Dr. Wheeler K. McGregor and Dr. Christian Parigger. Appreciation is also expressed to Dr. Robert A. Reed for his advice and contributions to this thesis and to Aerospace Testing Alliance near Tullahoma, TN for the opportunity to pursue this graduate degree.

Abstract

Point source extraction is critical to proper analysis of images containing point sources obtained by focal plane array cameras. Two popular methods of extracting the intensity of a point source are aperture photometry and point spread function fitting. Digital aperture photometry encompasses procedures utilized to extract the intensity of an imaged point source. It has been used by astronomers in various forms for calculating stellar brightness. It is also useful for doing analysis of data associated with other unresolved radiating objects. The various aperture photometry methods include the two-aperture method, aperture correction, and growth curve method.

The growth curve method utilizes integrated irradiance within an aperture versus growing aperture size. Signal to noise ratio, imperfect backgrounds, moving and off centered targets, and noise structure are just a few of the items that can cause problems with point source extraction. This thesis presents a study of how best to apply the growth curve method.

Multiple synthetic image sets were produced to replicate real world data. The synthetic images contain a Gaussian target of known intensity. Noise was added to the images, and various image related parameters were altered. The growth curve method is then applied to each data set using every reasonable aperture size combination to calculate the target intensity. It will be shown that for different types of data, the most optimal application of the growth curve method

can be determined. An algorithm is presented that can be applied to all data sets that fall within the scope of this study will be presented.

Table of Contents

1. Introduction 1

2. The Growth Curve Method 6

3. Approach 14

4. Findings and Results 22

5. Future Improvements 28

6. Summary 30

References 32

Appendix 35

Vita 50

List of Figures

Figure 1: Growth Curve Apertures 7

Figure 2: Flat Background Growth Curve 9

Figure 3: Image with Noise and Apertures 10

Figure 4: Background Noise Growth Curve 10

Figure 5: Growth Curves for Various S/N Ratios 12

Figure 6: Noise Effects at Large Aperture Size 13

Figure 7: Synthetic Scene Generation 15

Figure 8: FWHM Maximum Variation 16

Figure 9: Gaussian Centroid Offset 16

Figure 10: Signal to Noise Variation 18

Figure 11: 100 Growth Curves For One Data Set 19

Figure 12: Extracted Intensity with Algorithm Application 27

List of Tables

Table 1: Image Parameters 36

Table 2: Offset Comparison FWHM-1.5 S/N-100 36

Table 3: Offset Comparison FWHM-2.5 S/N-100 37

Table 4: Offset Comparison FWHM-1.5 S/N-25 38

Table 5: Offset Comparison FWHM-2.5 S/N-25 39

Table 6: FWHM Comparison S/N-100 Offset-0 40

Table 7: FWHM Comparison S/N-25 Offset-0 42

Table 8: S/N Comparison FWHM-1.5 Offset 0..... 44

Table 9: S/N Comparison FWHM-4 Offset 0 46

Table 10: Algorithm Application Results 48

1. Introduction

Remote sensing involves gathering information about the physical world by detecting and quantifying signals composed of radiation, particles, and fields emanating from objects located beyond the immediate vicinity of the sensor device. The information collected by the sensors can be placed into one of three categories: spatial, spectral, and intensity information. Some sensors produce data that fall into two or all three categories. For example, an imaging radiometer produces both spatial and intensity data, but since it can have spectral dependent sensitivity, spectral data is produced as well. This thesis will focus on systems that produce images. Digital imagers consist of a variety of materials and operate in numerous electromagnetic bands. Regardless, these instruments all produce an image that consists of an array of pixels each representing the amount of incident radiation present during the time of exposure [1].

Imagery can consist of extended resolved sources or unresolved point sources. In order to analyze point source imagery it is typical to extract the total irradiance of the target. There are a variety of techniques for extracting point source intensity, each with respective strengths and weaknesses.

One popular method for extracting point source intensity is point spread function (PSF) fitting. The PSF describes the response of an imager to a point source, and is sometimes referred to as the blur function. An image produced by the imaging system is simply the convolution of the object being imaged with the PSF of the system. This is true for unresolved point sources or resolved

extended objects. A PSF can also be thought of as a modulation transfer function (MTF) in the spatial domain. The MTF is the modulus of the optical transfer function (OTF) [2]. PSF fitting is a viable point source extraction method, but requires accurate knowledge of the system PSF. In addition, there can be no apparent motion within the time scale of the integration time of the sensor. The PSF overlays the image, and the position and amplitude are adjusted until the difference between the two are minimized. The extracted signal is then taken to be the summation or amplitude of the adjusted PSF [3]. In general, varying conditions may induce ambiguities that are difficult to resolve by resorting to the PSF approach only. In some cases, the PSF is simply unknown. In others, the PSF may have changed. A satellite that underwent characterization on the ground may exhibit different parameters once on orbit. Still in other cases the target may be constantly moving and any known PSF will not apply due to the blur related to the motion [4].

Aperture photometry methods tend to be more useful for recorded data. With a perfect image, without noise and a background of zero, one could simply apply a digital aperture of any size as long as it effectively contains the entire signal from the target. Since the point source image extends beyond digital windows, it is not possible to completely contain it. A similar issue is encountered when measuring the beam width of a laser. A criterion commonly used with lasers is D4σ, which is a beam diameter of four sigma [5]. In this case, the digital aperture should be at least six sigma wide, or three sigma radius, to capture

more than 99% of the signal. To be clear, a digital aperture is simply a defined region of the image containing the point source [6]. A summation of the signal from all pixels within that aperture would be the extracted intensity of the target. Of course, it is not that easy with actual recorded data. One subtype of aperture photometry is the two-aperture method. Two digital apertures defining the integration area are centered on the point source. Each aperture is large enough to effectively contain the complete point source out to three sigma with one aperture larger than the other. The integrated intensities of the two apertures are then compared [7]. Since one aperture is larger than the other, it will collect more background. The comparison results in two linear equations and two unknowns. One of these unknowns is the point source intensity. The equations are

$$I_1 = N_1 \times BG + I_0 \tag{1}$$

$$I_2 = N_2 \times BG + I_0 \tag{2}$$

where I_1 and I_2 are the integrated signal, N_1 and N_2 are the number of pixels contained within the two apertures, *BG* is the uniform background level, and I_0 is the actual intensity of the point source. Subtracting the two equations yields the background value, *BG*, which can be substituted into one of the original equations to find the point source intensity.

$$I_0 = I_1 - N_1 \frac{I_2 - I_1}{N_2 - N_1} \tag{3}$$

One advantage of this method is that it does not require a well-defined PSF. It simply requires that both apertures be larger than three sigma of the point source

itself. The two-aperture method can be thought as of the growth curve method in its most simple form [8].

Noise must be considered when using any aperture photometry method. Larger apertures will integrate more noise, which will introduce uncertainty with point source intensity calculations. In the case of white noise, the image noise is proportional to the square root of the number of pixels. For pink or red noise, the noise level increases more quickly with aperture size. The color of the noise refers to its power spectral distribution. White noise has a flat distribution while pink and red noise have a distribution proportional to 1/f and $1/f^2$, respectively [9]. When noise is present, the smallest aperture that still effectively contains the point source will be the most optimal. However, if the apertures get too small, the calculated signal will be truncated, producing an underestimate of the actual intensity of the target [7]. Nevertheless, there is a method that allows even smaller apertures to be used.

The aperture correction method allows us to use apertures that are smaller than the point source itself. The aperture correction method uses one aperture that is comparable to the full width half maximum (FWHM) of the point source image and a correction factor. The correction factor is based on the PSF shape. For example, if the point source is a Gaussian, and the aperture size is the same as the FWHM, only 76% of the energy will lie within the aperture. A correction factor of approximately 1.3 would be applied to the truncated intensity in order to find the actual intensity. Alternatively, the growth curve method (see

Chapter 2) could be applied to an uncrowded target with high signal to noise in order to find the total intensity. Applying the reduced aperture to that same target and comparing with the total intensity will yield the correction factor to be applied to other targets which may be crowded with other sources which maybe very faint [10].

Crowding is not a problem typically encountered when analyzing data not related to stellar fields. Also, the PSFs for many of the imaging systems that produce the data are not well known. Point sources may exhibit motion due to tracking error or motion of the target itself, thus rendering any technique requiring a stable PSF useless. For these reasons, much of the data lends itself to the growth curve method of aperture photometry.

2. The Growth Curve Method

The need for the growth curve method lies within signal to noise arguments. Obviously, a larger digital aperture will contain more radiation flux than a smaller one. However, the rate at which the signal grows with increasing aperture size declines as the wings of the point source approach zero intensity. At the same time, noise in the measurement grows rapidly with increasing aperture size. Contributions to this noise can include random errors in readout, Poisson shot noise, flat-field errors, etc. As a result, the signal to noise ratio (S/N) reaches an optimal value at some intermediate aperture size. This aperture may or may not be large enough to capture the flux within three sigma from the source. Also, this optimum aperture size will be dependent on signal intensity. One way to improve this method is to add another, larger concentric aperture [3]. This is the basis for the two-aperture method discussed in the previous chapter.

A more powerful method is to measure the flux in several concentric apertures and calculate the flux difference between successive apertures. Each aperture is centered on the point source as illustrated in Figure 1. The flux contained within each aperture is plotted versus aperture size, producing the so-called growth curve. The growth curve will grow until the aperture is large enough to capture three sigma of the present signal and will become linear with a slope based on the image background. [7]

Figure 1 contains a Gaussian point source with a total intensity of 100 counts. The FWHM of the Gaussian is three pixels. Nine digital apertures ranging

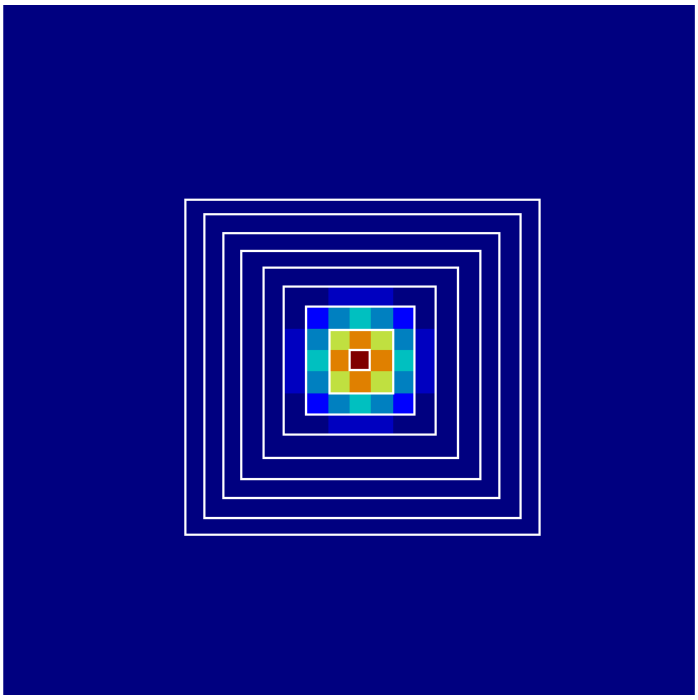

Figure 1: Growth Curve Apertures

in size from 1x1 to 17x17 have been applied. The background level is perfectly flat at 0.25 counts. Figure 2 illustrates the growth curve resulting from the image. The red line is a linear fit that has been applied to the portion of this curve corresponding to apertures beyond three sigma. The intercept is the intensity of the signal. In this case, the intercept is exactly 100 counts as expected. This result was easily achieved since the background was perfectly flat and absent of noise. Alternatively one could have subtracted 0.25 from the entire image and found the summation of every pixel in the image. The summation would be exactly 100 for this example.

The simulated flux in this example was completely contained within the 9x9 digital aperture. Applying a linear fit to any number of points along the growth curve corresponding to apertures 9x9 or larger would produce an intercept of 100 counts. In this ideal case, the only consideration is the minimum aperture size that defines the first data point for the linear fit. Once noise is considered, the task of selecting apertures for the linear fit becomes more difficult.

Figure 3 is another Gaussian point source image with the same attributes as the one in Figure 1. However, this image has been modified with noise. The signal to noise ratio is 200. Even with a relatively high signal to noise ratio, the growth curve in Figure 4 illustrates potential issues. The curve is not perfectly linear as it was in Figure 2. The red line is a linear fit to the points related to apertures 9x9 through 17x17. The linear fit is accomplished by using the method

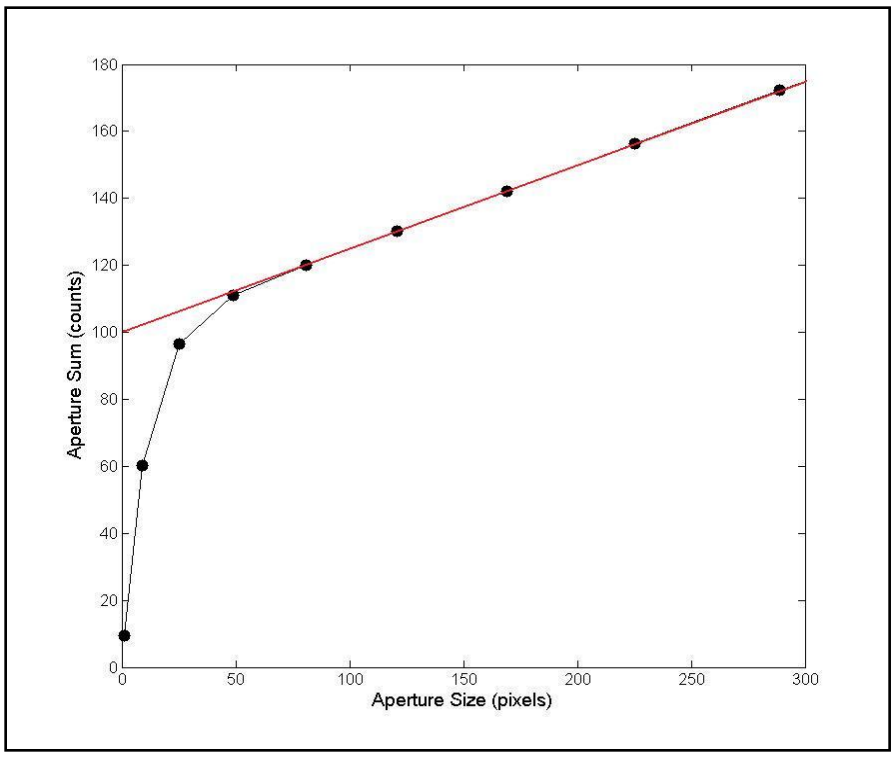

Figure 2: Flat Background Growth Curve

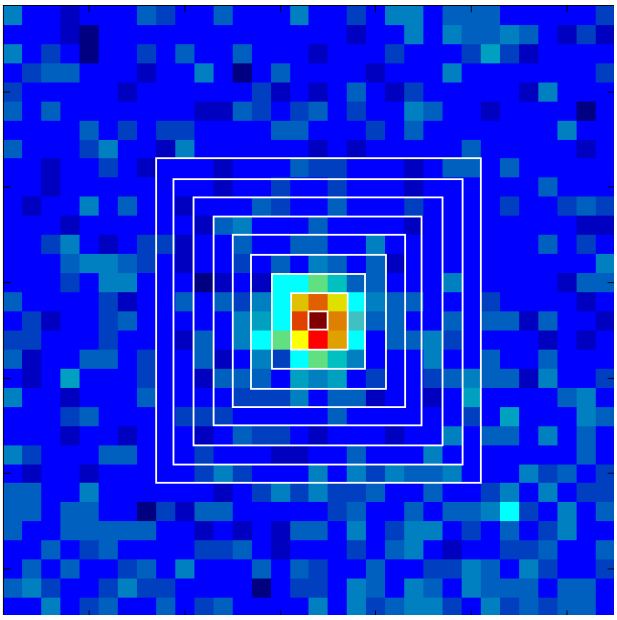

Figure 3: Image with Noise and Apertures

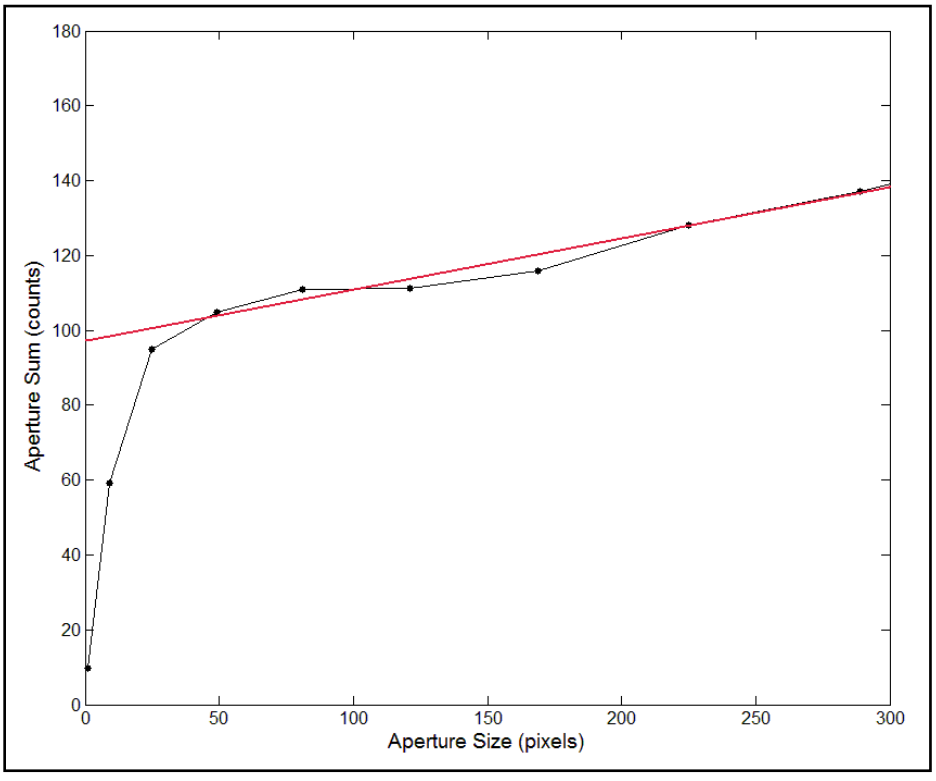

Figure 4: Background Noise Growth Curve

of least squares. This fit yielded an intercept of approximately 97. The introduction of noise has resulted in a 3% loss in total extracted intensity.

Figure 5 illustrates the effects various signal to noise ratios can have on growth curves. Each curve results from an image with an integrated intensity of 100 counts, but with signal to noise ratios varying from 500 down to 5. Figure 6 shows the uncertainty in measurements at larger apertures. The growth curve is the average of 100 curves produced from 100 synthetic images with noise. One sigma error bars are also shown. As the aperture gets larger, the uncertainty in the measurement goes up as well. This effect becomes even more evident as the signal to noise ratio goes down.

Typically, when presented with actual data to analyze, the user will produce a growth curve for initial assessment. The best place to apply a linear fit is then determined simply by viewing the growth curve. This has been successful in the past, but can be tedious and is based more on user intuition than actual analysis of the imagery. This can cause problems if the linear fit is applied to apertures that may be too small or unnecessarily large. A way to avoid improper point source extraction is by properly understanding the behavior of growth curves by applying them to a variety of data with known source intensities. The results can be analyzed in order to find an optimized solution for specific types of data or even larger subsets of data that may be encountered.

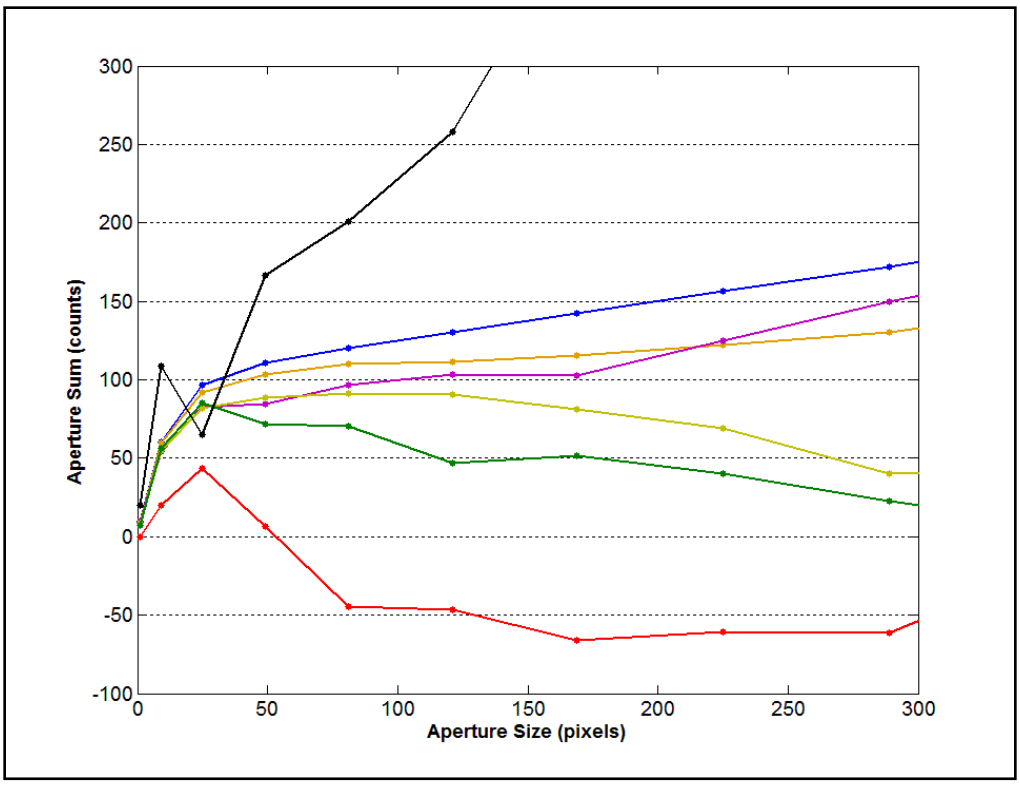

Figure 5: Growth Curves for Various S/N Ratios

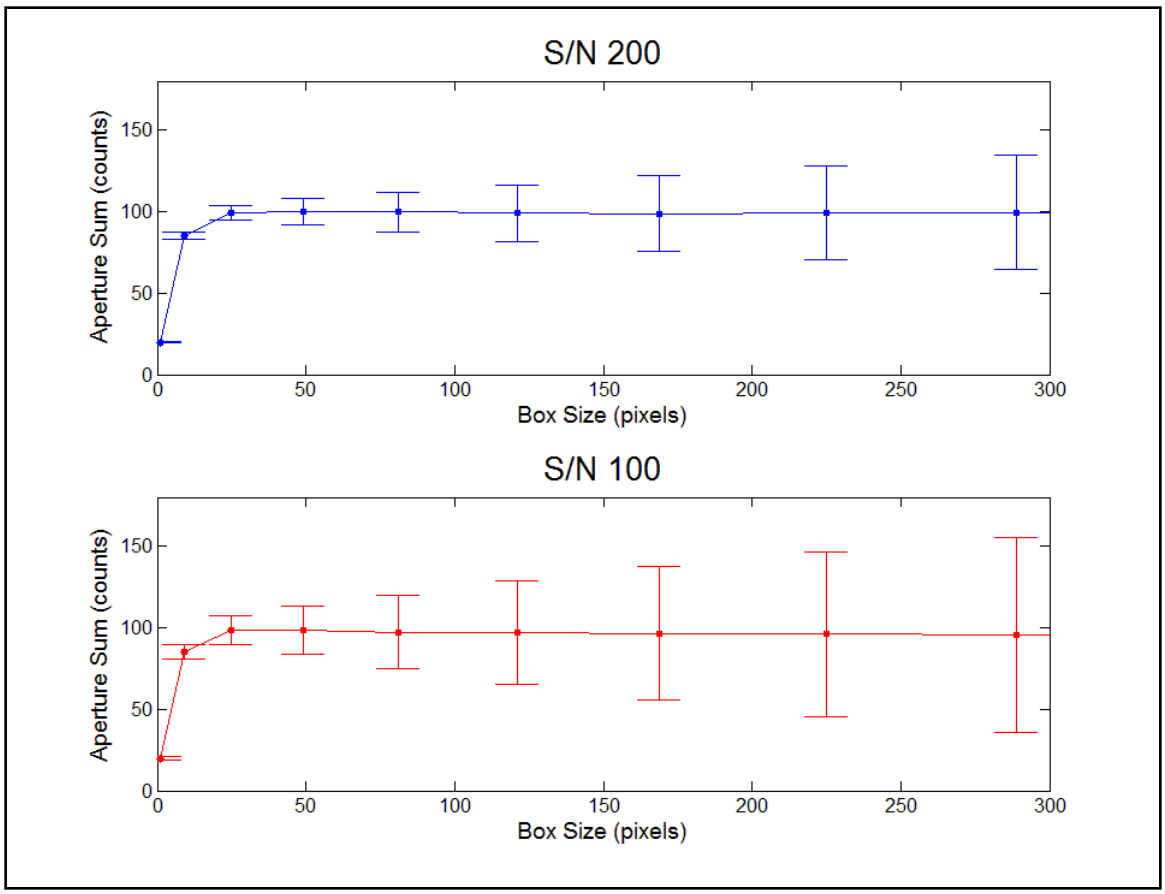

Figure 6: Noise Effects at Large Aperture Size

3. Approach

For this analysis, multiple synthetic data sets were created. Each set contains 100 images of a Gaussian point source. A Gaussian function is frequently used to model a PSF [11]. Each point source was normalized to have an integrated intensity of 100 counts. Signal to noise, FWHM, and centroid offset all vary in each data set. In the end, 84 different data sets were created resulting in 8,400 unique images to be analyzed. Each image was 32x32 pixels with the point source located in the center. All data creation and analysis were performed using MATLAB 7.8.0 (2009a).

Each image starts off as a two-dimensional (2-D) Gaussian function. The formula for a 2-D Gaussian is as follows

$$f(x,y) = Ae^{-[\frac{(x-x_0)^2}{2\sigma_x^2}+\frac{(y-y_0)^2}{2\sigma_y^2}]} \quad (4)$$

where σ is a spread parameter related to FWHM by formula 5, A is amplitude, and (x_0,y_0) is the Gaussian center location.

$$FWHM = 2\sqrt{2ln2}\sigma \quad (5)$$

For this analysis, σ_x and σ_y are equal producing a circular Gaussian. A Gaussian function is spatially smooth; however, imaging systems collect data that is spatially discrete. The result is an image that can be represented by the convolution of the original Gaussian signal and the discrete Gaussian kernel [12]. The first two frames of Figure 7 illustrate a smooth Gaussian and its discrete counterpart image. The third frame displays the addition of noise, which will be discussed later in this chapter.

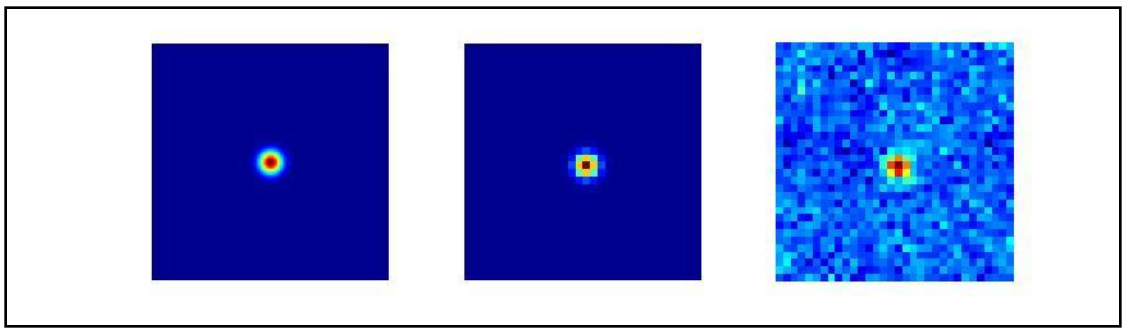

Figure 7: Synthetic Scene Generation

Six values for the FWHM of the Gaussian were used to create the data sets. The values were 1.5, 2, 2.5, 3, 4, and 5. These values were chosen to reflect the same values that are commonly encountered in imagery data. Figure 8 illustrates a Gaussian with FWHMs of 1.5, 2, and 2.5. Each image is on the same color scale to show the relative change. Even with the same signal to noise, a high FWHM can cause more of the signal to be lost to noise.

The centroid offset is another parameter varied for this study. Centroid offset is the location of the centroid based on the center of a pixel. In this case, the offset will be a single number indicating the distance to the right and below the center of the pixel. An offset of zero indicates that the Gaussian centroid is exactly centered on a pixel and is symmetrical. An offset of 0.2 indicates the centroid is located at point 0.2 pixels to the right and 0.2 pixels down. An offset off 0.5 indicates the centroid is located at the junction of four pixels. Figure 9 illustrates centroid offsets of 0, 0.2, and 0.4, which are the offsets used in this experiment.

Noise is the most critical aspect of the synthetic data sets. The noise introduced in this experiment has a power spectral density of the form

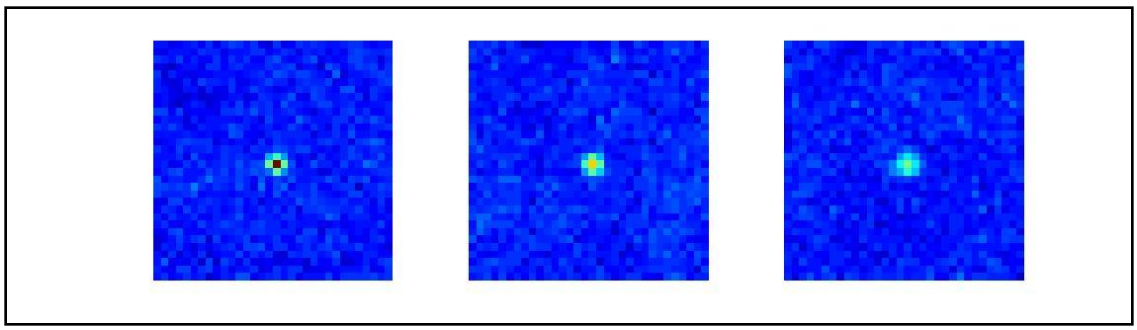

Figure 8: FWHM Maximum Variation

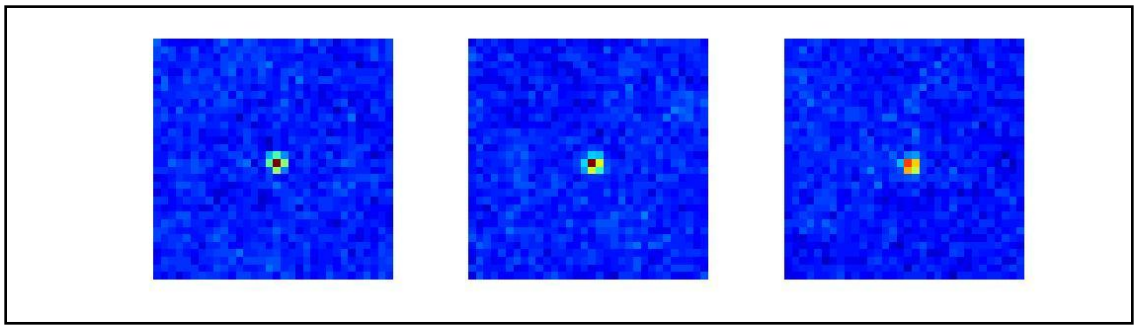

Figure 9: Gaussian Centroid Offset

$$S(f) \propto \frac{1}{f^{\alpha}} \tag{6}$$

where *f* is frequency and $0 < \alpha < 2$. White noise corresponds to $\alpha = 0$, which was used in this experiment to simulate thermal noise. So called “pink noise” corresponds to $\alpha = 1$, and was used to simulate noise from other sources related to the sensor electronics. The power spectral density is the Fourier transform of the noise signal and is measured in units of Watts/Hz [13]. A separate 32x32 noise frame was created for each of the 8,400 images. The noise frame was created by adding a pink noise frame and a white noise frame with a multiplicative weighting factor. White noise usually dominates the pink noise to some degree in the data of interest. The weighting factor used for this experiment was two. This resulted in a white noise frame with a standard deviation double that of the pink noise frame. The frames were added together and then scaled such that the standard deviation of the resulting frame was the desired fraction of the target intensity. Figure 10 shows frames with various signal to noise ratios resulting from this process. The ratios represented are 100, 50, and 25. The point source in Figure 10 has a FWHM of 1.5 pixels.

The basis for creating the noise is the pseudo-random number generator utilized by MATLAB. The function “randn” returns pseudo-random numbers with a normal distribution. The sequence of numbers generated by randn utilize MATLAB’s default number stream. These values work well for the Monte Carlo type of simulation executed in this experiment. The function randn produces the 32x32 noise array which can be filtered in the frequency domain to produce the

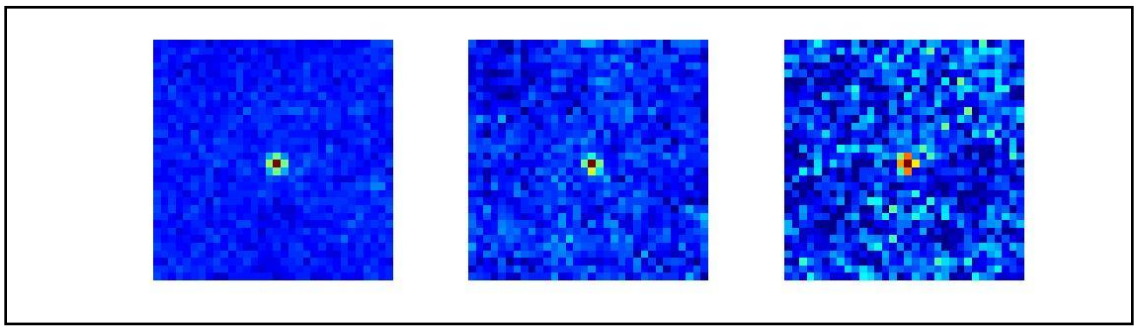

Figure 10: Signal to Noise Variation

white and pink noise frames [14]. The “randn” function works well for a single workstation. However, in order to expand this study and use parallel computing, a different pseudo-random number generator would need to be utilized. The Scalable Parallel Pseudo Random Number Generator (SPRNG) would work well in this case [15].

Once the noise frame is created, it is added to the Gaussian frame with the appropriate FWHM and centroid offset. The result is an image closely approximating actual data produced by an imaging system. The process is repeated 100 times producing 100 images with the same FWHM, centroid offset and signal to noise ratio, but with different noise patterns resulting from the pseudo-random number generator. All parameters included in the study are listed in Table 1. All tables are located in Appendix A.

The analysis of each data set begins with producing a growth curve for each of the 100 images. Figure 11 illustrates 100 growth curves for the data set representing a signal to noise ratio of 100, a FWHM of 2, and an offset of 0. The

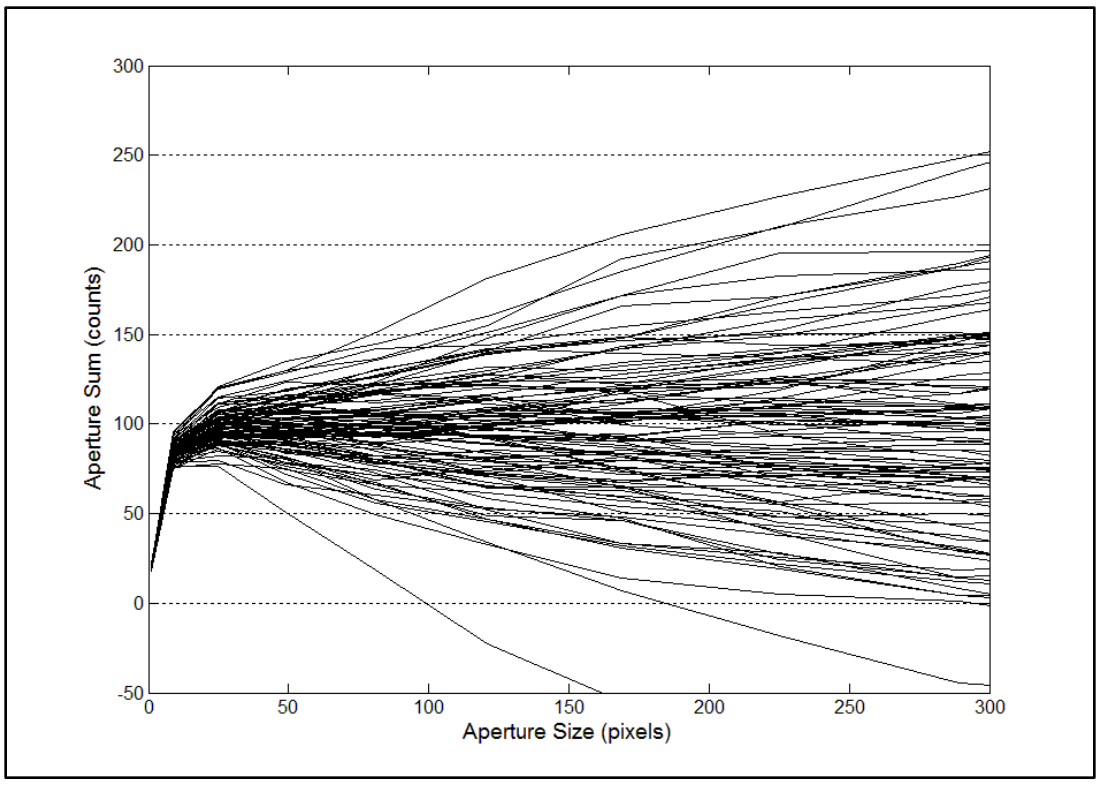

Figure 11: 100 Growth Curves For One Data Set

positive and negative slopes are a result of imperfect background corrections resulting in locally positive or negative backgrounds. The calculated growth curves resulted from aperture sizes starting with 1x1 and ending with 21x21. A linear fit was calculated for every possible start and stop point within these two aperture sizes. For example, if the start and stop point are 5x5 and 11x11, then a linear fit is applied to the points along the growth curve corresponding to aperture sizes 5x5, 7x7, 9x9, and 11x11. This calculation would be performed on all 100 growth curves resulting in 100 extracted intensities for the point source for that particular combination of start and stop apertures. A mean and standard deviation were calculated based on these values. In the example used to produce Figure 11, a linear fit to the points between and including 5x5 and 11x11 resulted in a mean of 99 and a standard deviation of 7.3. Considering the actual intensity is 100 counts, this result is very accurate. However, it may not be the best result one could achieve using the same 100 growth curves.

With aperture sizes between 1x1 and 21x21, there are 55 possible start and stop combinations for calculating a linear fit. The combinations go as follows. 1x1 to 3x3, 1x1 to 5x5, 1x1 to 7x7…15x15 to 21x21, 17x17 to 21x21, 19x19 to 21x21. All 55 combinations were applied to the 100 growth curves for each case. This resulted in 55 unique sets of average intensities and the respective standard deviations. A ranking system was developed in order to quickly determine which aperture start and stop combination works best for each

data set. The ranks were based on which combinations produced the lowest value for the following formula created for this study,

$$score = w\left|1 - \frac{I_0}{100}\right| + \left|\frac{\sigma}{I_0}\right| \quad (7)$$

where I_0 is the average calculated intensity from one hundred growth curves, σ is the standard deviation of the extracted intensities, and w is a weighting factor. The first term in the equation after the weighting factor represents the percent difference from the expected extracted intensity of one hundred counts. The second additive term is the standard deviation of the intensity calculations scaled by the average calculated intensity. A perfect score in this case would be zero. A score of zero indicates all one hundred growth curve measurements yielded an extracted intensity of one hundred counts.

The equation allows us to find the most accurate answer with the highest precision. It simply adds the accuracy and the precision of the measurement. The accuracy is given a weighting factor to ensure that accuracy has priority over precision. For this study, a weighting factor of three was applied, such that accuracy played a major role in the rankings but still allowed precision to have some influence. The result of this analysis is presented in the next chapter.

4. Findings and Results

After completing all calculations, a Microsoft Excel file was created to save all of the data. Each tab of the spreadsheet contained a single test case with all 55 aperture start and stop combinations. For each combination the spreadsheet has the start aperture, stop aperture, average extracted intensity, standard deviation, a score resulting from the equation on the previous page, and the rank of the score among the other aperture combinations for that 100 frame dataset. Each table was sorted leaving the best aperture combinations at the top of each tab. All tables referred to in this section are available in Appendix A.

The first image parameter analyzed was the centroid offset. Intuitively, offsets that are small (less than 1/3) as compared to the FWHM should have little effect other than perhaps increasing the size of the minimum aperture since the offset may move the wings outside of the optimal minimum aperture for a target centered on a pixel. In this case, the evidence supports the intuition. Table 2 lists the five most optimal aperture combinations for all 3 offsets for data with a signal to noise ratio of 100 and a FWHM of 1.5 pixels. Data with an offset of zero and 0.2 agree well. One slight difference of note is that three of the top five start apertures associated with zero offset are 3x3 while only two are for the offset 0.2 data. For an offset of 0.4, all starting apertures are 5x5 indicating that a larger starting aperture is required for this particular data set. This makes sense because an offset of 0.4 is a larger percentage of the 1.5 pixel FWHM.

The same comparisons were made for a 2.5 FWHM. As seen in Table 3, the data associated with offsets of zero and 0.2 are the same in that they both have three starting apertures of 7x7 and two of 5x5. For data with an offset of 0.4, there were four 7x7 start apertures and only one 5x5 start aperture, indicating the offset had a slight effect similar to the previous data with a FWHM of 1.5. Again, this makes sense because the 0.4 offset is a lesser percentage of a 2.5 FWHM. Tables 4 and 5 show the same comparisons from above, but with a reduced signal to noise ratio of 25. These data exhibited similar trends to the data with a signal to noise ratio of 100, but to a lesser degree.

The next parameter examined was FWHM. Again, if intuition were applied, one would expect the minimum aperture to increase with FWHM. As before, the data agrees with intuition. Table 6 shows the five most optimal start and stop aperture combinations for a signal to noise ratio of 100 and a centroid offset of zero with FWHM varying between 1.5 and 5. The start aperture sizes clearly increase along with the FWHM. In fact, a trend emerges from this particular example. The best start aperture size is one that is twice the FWHM max or one step larger. For a FWHM of 1.5, the five most optimal start apertures are either 3x3 or 5x5. For a FWHM of 3, all five optimal start apertures are 7x7 pixels.

Table 7 displays the same comparison as Table 6, but with signal to noise ratio reduced to 25. In this case, the optimal start aperture still increases with FWHM, but the increase in noise seems to keep them somewhat smaller than in the previous example. The FWHM values of 1.5 through 3 still follow the same

trend as before, however the trend breaks down beyond that. For a FWHM of 4, one would expect the best start aperture to be 9x9, however only the fifth most optimal start aperture is 9x9. The rest are a smaller 7x7. This implies that lower signal to noise ratios have small optimal apertures, as expected from earlier noise discussions. Also of note, the average extracted intensity trends downward as FWHM increases. The average extracted intensity for the top five aperture combinations with a FWHM of 1.5 is 98.2. For a FWHM of 5, the average extracted intensity is only 92.3. This is probably due to the wings of the signal being lost to noise or truncation due to the smaller aperture sizes.

Finally, trends related to signal to noise ratio were examined. The ratios included were 100, 75, 50, 25, 10, 5, and 2. Table 8 shows the five most optimal start and stop aperture combinations for a FWHM of 1.5, a centroid offset of 0, and all signal to noise ratios. The optimal start aperture size shows no dependence on signal to noise ratio. The dominant starting aperture is 3x3 for this case. The optimal stop apertures however do exhibit a trend related to the signal to noise ratio. As the signal to noise ratio goes down, the optimal stop apertures get smaller. For a signal to noise ratio of 100, four of the five optimal stop apertures are 11x11 or higher, indicating better results using more apertures for computing the linear fit. For a signal to noise ratio of 25, four of the five optimal stop apertures are 9x9 or lower, indicating better results using fewer apertures for computing the linear fit.

Table 9 is the same as Table 8 except the FWHM is 4. For this case, the optimal starting apertures show a slight trend toward smaller sizes with an increase in signal to noise ratio. In this case, data at or below a signal to noise ratio of 25 are questionable since the standard deviations of the measurements are 50% or more of the extracted intensity. This was also true for data at or below a signal to noise ratio of five for a FWHM of 1.5. As before, the optimal stop aperture size reduces as the signal to noise ratio goes down.

The last step of this analysis is to utilize all of the results to produce an algorithm that can be applied to any data set within the scope of this study. Based on the findings so far, the framework of an algorithm can be formed. The minimum starting aperture should be one step higher than double the FWHM. If it is 1.5, then the starting aperture should be 5x5. If it is 4, then the starting aperture should be 9x9. While the stopping aperture should be related to the signal to noise, it can be difficult to calculate it for some data sets. It seems simply cutting off the linear fit with a stop aperture of three positions higher than the start aperture will suffice for most cases. In the case of a 1.5 FWHM, this means the stop aperture would be 11x11. For a value of four, it would be 15x15. The results of universally applying this algorithm to all data sets in this study can be seen in Table 10. Data in which the signal to noise ratio is too low have been omitted. Applying this algorithm works surprisingly well and requires nothing more than an estimation of the FWHM of the image. Of the 84 cases, 60 had sufficient signal to noise for proper analysis. Applying the algorithm outlined

above consistently yielded high-ranking results from each data set. In fact, applying the algorithm to 17 of the 60 cases yielded either the first or the second most optimal solution. The median rank for all 60 cases was 4. Figure 12 shows the extracted intensities yielded by applying the algorithm universally to all 60 cases. In each case, one hundred intensities were extracted from one hundred growth curves. The mean and standard deviation of the intensities were calculated for each case. One sigma error bars are included. The average extracted intensity for all cases was 99 with an average standard deviation of 23. Table 10 lists the results from all 60 cases that are illustrated in Figure 12. Having a general algorithm this successful on multiple types of image data can be very useful when processing large quantities of data.

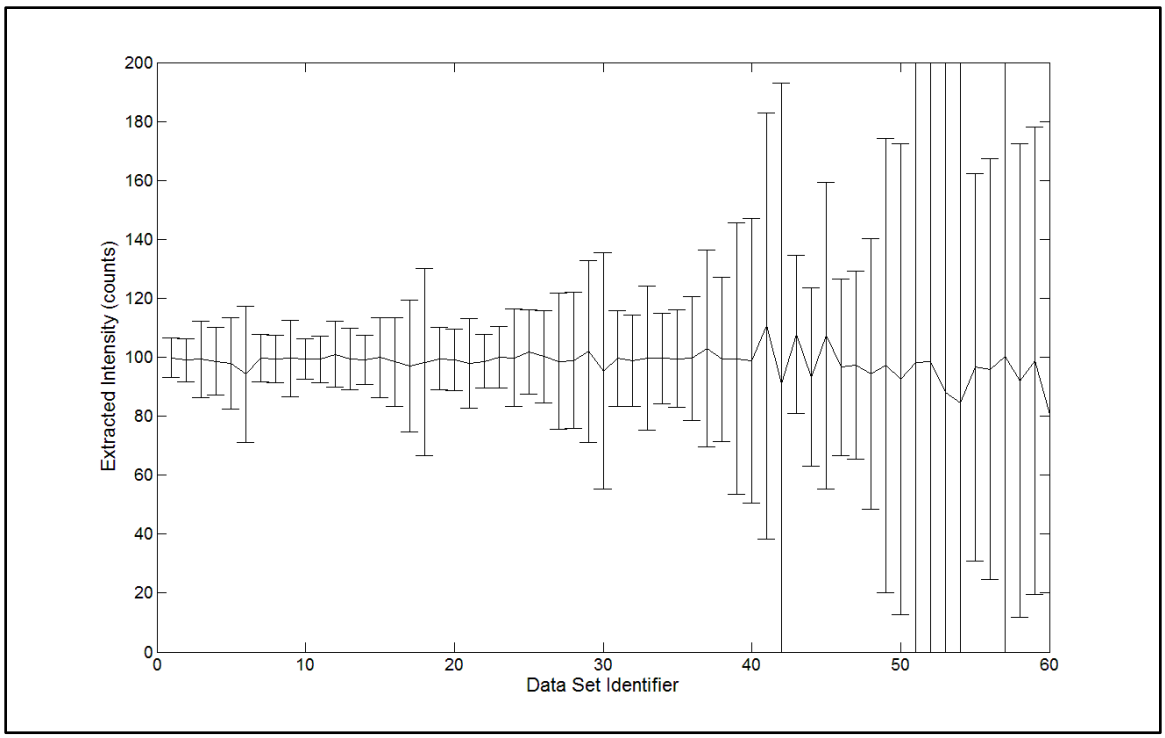

Figure 12: Extracted Intensity with Algorithm Application

5. Future Improvements

The analysis in this thesis established trends based on image parameters. These trends are helpful in determining the best application of the growth curve method. However, there is room for improvement. There were unexpected inconsistencies between data sets with similar image parameters. One solution could be to expand the number of frames per data set beyond 100. Perhaps doing 1,000 frames per data set would have yielded better results, but the tradeoff would have been the time required to do so. Processing the 8,400 frames took approximately 16 hours of computer processing time. Increasing the frame number tenfold would increase the computation time similarly. An alternative would be to use parallel computing in order to increase throughput.

Another area for improvement would be to test non-circular Gaussian targets. Many data of interest contain objects that are blurred due to tracking jitter or simply the object moving. The result may likely be that the minimum aperture is related to the broader of the two Gaussian widths, but it may still be worth closer inspection.

Investigating profiles that are not Gaussian is also an area for future improvement. Though a Gaussian profile is a good approximation for most imager data, it would still be interesting to explore other profiles such as a Lorentzian, a combination of different curves, or a shape that is unique to a particular imaging system.

Also, an exploration of the effects of bad pixels would be valuable. Typically, a bad pixel is corrected by replacing it with the median value of the surrounding pixels. This works well for extended sources, but can have a drastic effect on a point source. A study on how a corrected bad pixel affects the intensity extracted using the growth curve method for various image parameters would be a welcome addition to the analysis presented here.

Filtering the images in Fourier-transform space should also be explored. The study presented in this thesis could be repeated after applying a noise filter to all images. A Savitzky-Golay smoothing filter would be ideal for this application since it may preserve the original features that other smoothing techniques can alter [16]. Filtering may reduce the standard deviation of the measurement, but accuracy should be carefully examined after applying any filtering technique.

Finally, an analysis of real world data would be valuable. Due to sensitivity of the imaging systems and all data produced from them, no real world data analysis were included in this thesis.

6. Summary

The intent of this thesis was to show that the growth curve method of aperture photometry could be optimized based on image criteria. Unlike point spread function (PSF) fitting and other forms or aperture photometry, the growth curve method does not require a detailed PSF of the imaging system. It is also advantageous when analyzing data in which the point source may be blurred due to tracking errors or target motion.

In all, 84 synthetic image sets containing 100 images each were created for examination. Each image set contained a Gaussian point source and had various image parameters altered. The variable parameters were signal to noise ratio, full width half maximum of the Gaussian, and the centroid offset. Growth curves were calculated for every single image produced, and a linear fit was applied to each curve with every possible aperture start and stop combination possible between 1x1 and 21x21.

The resulting data were analyzed for how the optimal application of the growth curve is affected by image parameters. It was found that the optimal starting aperture was directly related to the full with half maximum (FWHM), loosely related to the centroid offset, and not related to the signal to noise ratio. The optimal stop aperture was directly related to the signal to noise and FWHM. Centroid offset had no effect on the optimal stop aperture size.

Finally, an attempt was made to create a general algorithm that could be applied to data of this type. An algorithm that works well is starting the linear fit at

the aperture that is one step above twice the FWHM and ending it at the aperture that is three steps above it. Utilizing this algorithm will provide accurate results while not sacrificing the time to examine a new growth curve each time. Time is also saved by not performing an optimization routine on every single data set to be analyzed. The presented algorithm works well for data within the scope of this study. However, the algorithm may need to be applied with care and/or modified prior to application to different data sets.

References

[1] Short, N. M., **The Remote Sensing Tutorial**. Retrieved March 26, 2010, from http://rst.gsfc.nasa.gov/

[2] Hecht, E., **Optics,** 4th Edition, Pearson Education, Boston, MA, 2001.

[3] Howell, S. B., **Handbook of CCD Astronomy,** 2nd Edition, Cambridge University Press, New York, NY, 2000.

[4] Lam, E.Y. and Goodman, J.W., *Iterative statistical approach to blind image deconvolution,* Journal of the Optical Society of America A, Vol 17, Issue 7, p. 1177-1184, 2000.

[5] Johnston, T.F., *Beam Propagation (M^2) Measurement as Easy as It Gets: The Four-Cuts Method,* Applied Optics, Vol 37, Issue 21, p. 4840-4850, 1998.

[6] Glass, I. S., **Handbook of Infrared Astronomy,** Cambridge University Press, New York, NY, 1999**.**

[7] Stetson, P. B., *On the Growth Curve Method for Calibrating Stellar Photometry with CCDs*," Society of the Pacific Conference Series, Vol 102, p. 932, 1989.

[8] Reed, R. A., personal communication, March 2010.

[9] Henning, G.B., Bird, C. M., Wichmann, F.A., *Contrast discrimination with pulse trains in pink noise*, Journal of the Optical Society of America A, Vol 19, Issue 7, p. 1259-1266, 2002.

[10] Howell, S. B., *CCD Growth Curves: Application To Faint and Crowded Point Sources,* Astronomical Society of the Pacific Conference Series, Vol 8, p. 312, 1989.

[11] Claxton, C. D. and Staunton, R. C., *Measurement of the point-spread function of a noise imaging system,* Journal of the Optical Society of America A, Vol 25, Issue 1, p. 159-170, 2008.

[12] Lindeberg, T., *Scale-Space for Discrete Signals,* IEEE Transactions of Pattern Analysis and Machine Intelligence, Vol 12(3), p. 234-254, 1990.

[13] Norton, P. M. and Karczub, D. G., **Fundamentals of Noise and Vibration Analysis for Engineers,** 2nd Edition, Cambridge University Press, New York, NY, 2003.

[14] The Math Works, Inc., **Image Processing Toolbox 5**, 13th printing, October 2005.

[15] Mascagni, M. and Srinivasan, A., *Algorithm 806: SPRNG: A Scalable Library for Pseudorandom Number Generation*, ACM Transactions on Mathematical Software, 26: 436-461, 2000.

[16] Savitzky, A., Golay, M., *Smoothing and Differentiation of Data by Simplified Least Squares Procedures*, Analytical Chemistry, vol 36(8), p. 1627–1639, 1964.

Appendix

Appendix A: Tables

Table 1: Image Parameters

FWHM	Signal to Noise	Offset
1.5	100, 75, 50, 25, 10, 5, 2	0, 0.2, 0.4
2	100, 75, 50, 25, 10, 5, 2	0, 0.2, 0.4
2.5	100, 75, 50, 25, 10, 5, 2	0, 0.2, 0.4
3	100, 75, 50, 25, 10, 5, 2	0
4	100, 75, 50, 25, 10, 5, 2	0
5	100, 75, 50, 25, 10, 5, 2	0

Tables 2-5 are the results of altering the centroid offset parameter.

Table 2: Offset Comparison FWHM-1.5 S/N-100

Offset 0					
Start	**Stop**	**Signal**	**StanDev**	**Score**	**Rank**
5x5	11x11	99.72	6.71	0.08	1
5x5	7x7	100.27	6.88	0.08	2
3x3	17x17	99.95	8.70	0.09	3
3x3	11x11	98.74	5.37	0.09	4
3x3	13x13	99.02	6.57	0.10	5
Offset 0.2					
Start	**Stop**	**Signal**	**StanDev**	**Score**	**Rank**
3x3	17x17	100.05	7.86	0.08	1
5x5	11x11	99.78	8.01	0.09	2
5x5	9x9	100.47	7.57	0.09	3
5x5	13x13	99.81	8.81	0.09	4
3x3	15x15	99.29	7.81	0.10	5
Offset 0.4					
Start	**Stop**	**Signal**	**StanDev**	**Score**	**Rank**
5x5	11x11	99.43	6.83	0.09	1
5x5	13x13	100.12	8.74	0.09	2
5x5	9x9	100.86	6.78	0.09	3
5x5	7x7	98.94	6.45	0.10	4
5x5	15x15	100.35	9.64	0.11	5

Table 3: Offset Comparison FWHM-2.5 S/N-100

Offset 0					
Start	**Stop**	**Signal**	**StanDev**	**Score**	**Rank**
7x7	11x11	100.21	10.80	0.11	1
5x5	15x15	99.13	9.43	0.12	2
7x7	9x9	100.58	11.16	0.13	3
7x7	15x15	99.70	12.78	0.14	4
5x5	13x13	97.93	7.89	0.14	5
Offset 0.2					
Start	**Stop**	**Signal**	**StanDev**	**Score**	**Rank**
5x5	15x15	98.90	9.41	0.13	1
7x7	13x13	99.56	13.08	0.14	2
5x5	21x21	98.88	12.33	0.16	3
7x7	9x9	98.69	11.90	0.16	4
7x7	15x15	99.19	13.56	0.16	5
Offset 0.4					
Start	**Stop**	**Signal**	**StanDev**	**Score**	**Rank**
7x7	11x11	100.57	11.42	0.13	1
5x5	15x15	98.90	9.76	0.13	2
7x7	13x13	101.03	11.19	0.14	3
7x7	17x17	100.17	14.19	0.15	4
7x7	15x15	101.42	11.43	0.16	5

Table 4: Offset Comparison FWHM-1.5 S/N-25

Offset 0					
Start	**Stop**	**Signal**	**StanDev**	**Score**	**Rank**
3x3	5x5	96.29	12.98	0.25	1
3x3	9x9	96.31	18.67	0.30	2
3x3	7x7	94.18	13.03	0.31	3
5x5	9x9	102.20	25.45	0.31	4
3x3	15x15	101.79	26.81	0.32	5
Offset 0.2					
Start	**Stop**	**Signal**	**StanDev**	**Score**	**Rank**
3x3	15x15	100.28	27.08	0.28	1
3x3	11x11	97.14	20.93	0.30	2
5x5	7x7	101.92	28.87	0.34	3
5x5	9x9	98.14	28.06	0.34	4
3x3	7x7	92.97	13.62	0.36	5
Offset 0.4					
Start	**Stop**	**Signal**	**StanDev**	**Score**	**Rank**
3x3	11x11	97.53	21.74	0.30	1
5x5	7x7	99.46	28.35	0.30	2
3x3	7x7	94.23	15.12	0.33	3
5x5	9x9	98.09	29.50	0.36	4
3x3	9x9	94.29	18.86	0.37	5

Table 5: Offset Comparison FWHM-2.5 S/N-25

Offset 0					
Start	**Stop**	**Signal**	**StanDev**	**Score**	**Rank**
5x5	11x11	100.34	28.66	0.30	1
5x5	13x13	101.97	31.30	0.37	2
5x5	9x9	96.42	26.36	0.38	3
5x5	7x7	93.62	24.47	0.45	4
7x7	9x9	100.71	44.99	0.47	5
Offset 0.2					
Start	**Stop**	**Signal**	**StanDev**	**Score**	**Rank**
5x5	13x13	100.32	34.78	0.36	1
5x5	9x9	96.06	26.50	0.39	2
7x7	11x11	99.93	48.28	0.49	3
5x5	15x15	104.80	36.87	0.50	4
5x5	11x11	94.31	32.59	0.52	5
Offset 0.4					
Start	**Stop**	**Signal**	**StanDev**	**Score**	**Rank**
5x5	13x13	97.36	28.59	0.37	1
5x5	15x15	100.40	38.70	0.40	2
7x7	11x11	100.94	44.00	0.46	3
5x5	17x17	102.20	46.06	0.52	4
5x5	9x9	92.77	31.84	0.56	5

Tables 6 and 7 are the results of altering the FWHM parameter.

Table 6: FWHM Comparison S/N-100 Offset-0

FWHM 1.5					
Start	**Stop**	**Signal**	**StanDev**	**Score**	**Rank**
5x5	11x11	99.72	6.71	0.08	1
5x5	7x7	100.27	6.88	0.08	2
3x3	17x17	99.95	8.70	0.09	3
3x3	11x11	98.74	5.37	0.09	4
3x3	13x13	99.02	6.57	0.10	5
FWHM 2					
Start	**Stop**	**Signal**	**StanDev**	**Score**	**Rank**
5x5	9x9	100.67	6.66	0.09	1
5x5	11x11	99.01	7.33	0.10	2
7x7	15x15	99.75	10.99	0.12	3
5x5	19x19	100.08	11.67	0.12	4
7x7	13x13	100.49	11.05	0.12	5
FWHM 2.5					
Start	**Stop**	**Signal**	**StanDev**	**Score**	**Rank**
7x7	11x11	100.21	10.80	0.11	1
5x5	15x15	99.13	9.43	0.12	2
7x7	9x9	100.58	11.16	0.13	3
7x7	15x15	99.70	12.78	0.14	4
5x5	13x13	97.93	7.89	0.14	5
FWHM 3					
Start	**Stop**	**Signal**	**StanDev**	**Score**	**Rank**
7x7	13x13	98.54	11.48	0.16	1
7x7	17x17	100.55	14.50	0.16	2
7x7	11x11	98.33	10.94	0.16	3
7x7	15x15	98.70	12.87	0.17	4
7x7	21x21	99.02	17.03	0.20	5
FWHM 4					
Start	**Stop**	**Signal**	**StanDev**	**Score**	**Rank**
9x9	11x11	99.88	17.53	0.18	1
9x9	17x17	99.28	18.28	0.21	2

9x9	13x13	97.86	15.56	0.22	3
11x11	13x13	99.73	21.81	0.23	4
9x9	15x15	98.50	18.63	0.23	5
FWHM 5					
Start	**Stop**	**Signal**	**StanDev**	**Score**	**Rank**
11x11	15x15	99.37	20.61	0.23	1
9x9	21x21	97.05	20.67	0.30	2
13x13	17x17	99.43	28.44	0.30	3
11x11	21x21	97.72	23.98	0.31	4
11x11	19x19	97.45	26.52	0.35	5

Table 7: FWHM Comparison S/N-25 Offset-0

FWHM 1.5					
Start	**Stop**	**Signal**	**StanDev**	**Score**	**Rank**
3x3	5x5	96.29	12.98	0.25	1
3x3	9x9	96.31	18.67	0.30	2
3x3	7x7	94.18	13.03	0.31	3
5x5	9x9	102.20	25.45	0.31	4
3x3	15x15	101.79	26.81	0.32	5
FWHM 2					
Start	**Stop**	**Signal**	**StanDev**	**Score**	**Rank**
5x5	11x11	99.33	27.80	0.30	1
5x5	7x7	98.47	30.82	0.36	2
5x5	9x9	97.09	28.39	0.38	3
3x3	17x17	97.68	37.00	0.45	4
3x3	13x13	93.45	24.44	0.46	5
FWHM 2.5					
Start	**Stop**	**Signal**	**StanDev**	**Score**	**Rank**
5x5	11x11	100.34	28.66	0.30	1
5x5	13x13	101.97	31.30	0.37	2
5x5	9x9	96.42	26.36	0.38	3
5x5	7x7	93.62	24.47	0.45	4
7x7	9x9	100.71	44.99	0.47	5
FWHM 3					
Start	**Stop**	**Signal**	**StanDev**	**Score**	**Rank**
5x5	15x15	98.73	36.12	0.40	1
7x7	9x9	99.55	41.29	0.43	2
5x5	13x13	95.90	35.43	0.49	3
7x7	13x13	98.75	48.29	0.53	4
7x7	11x11	106.11	41.94	0.58	5
FWHM 4					
Start	**Stop**	**Signal**	**StanDev**	**Score**	**Rank**
7x7	21x21	99.55	57.10	0.59	1
7x7	9x9	94.08	49.91	0.71	2
7x7	19x19	95.11	59.92	0.78	3
7x7	15x15	91.46	52.75	0.83	4

9x9	11x11	94.34	64.20	0.85	5
FWHM 5					
Start	**Stop**	**Signal**	**StanDev**	**Score**	**Rank**
9x9	13x13	96.04	62.12	0.77	1
7x7	21x21	94.56	64.17	0.84	2
9x9	17x17	93.44	65.58	0.90	3
9x9	21x21	96.72	87.85	1.01	4
5x5	19x19	80.68	52.26	1.23	5

Tables 8 and 9 are the results of altering the signal to noise parameter.

Table 8: S/N Comparison FWHM-1.5 Offset 0

S/N 100					
Start	**Stop**	**Signal**	**StanDev**	**Score**	**Rank**
5x5	11x11	99.72	6.71	0.08	1
5x5	7x7	100.27	6.88	0.08	2
3x3	17x17	99.95	8.70	0.09	3
3x3	11x11	98.74	5.37	0.09	4
3x3	13x13	99.02	6.57	0.10	5
S/N 75					
Start	**Stop**	**Signal**	**StanDev**	**Score**	**Rank**
5x5	7x7	99.79	10.41	0.11	1
5x5	11x11	99.46	10.46	0.12	2
5x5	9x9	99.13	9.98	0.13	3
3x3	13x13	98.12	7.65	0.13	4
3x3	17x17	99.13	10.83	0.14	5
S/N 50					
Start	**Stop**	**Signal**	**StanDev**	**Score**	**Rank**
3x3	7x7	97.51	8.04	0.16	1
5x5	7x7	99.02	13.18	0.16	2
3x3	9x9	97.03	8.87	0.18	3
3x3	15x15	98.61	13.76	0.18	4
5x5	9x9	101.68	13.86	0.19	5
S/N 25					
Start	**Stop**	**Signal**	**StanDev**	**Score**	**Rank**
3x3	5x5	96.29	12.98	0.25	1
3x3	9x9	96.31	18.67	0.30	2
3x3	7x7	94.18	13.03	0.31	3
5x5	9x9	102.20	25.45	0.31	4
3x3	15x15	101.79	26.81	0.32	5
S/N 10					
Start	**Stop**	**Signal**	**StanDev**	**Score**	**Rank**
3x3	9x9	97.47	42.06	0.51	1
3x3	7x7	94.43	38.47	0.57	2

3x3	13x13	102.97	57.40	0.65	3
5x5	9x9	100.22	66.64	0.67	4
3x3	5x5	90.67	36.65	0.68	5
S/N 5					
Start	**Stop**	**Signal**	**StanDev**	**Score**	**Rank**
3x3	7x7	101.36	73.39	0.76	1
3x3	9x9	107.98	85.12	1.03	2
3x3	5x5	88.15	67.80	1.12	3
3x3	11x11	93.09	106.36	1.35	4
5x5	9x9	104.42	132.58	1.40	5
S/N 2					
Start	**Stop**	**Signal**	**StanDev**	**Score**	**Rank**
3x3	5x5	102.97	194.25	1.98	1
3x3	7x7	92.77	182.75	2.19	2
3x3	9x9	111.44	215.18	2.27	3
1x1	7x7	66.29	94.78	2.44	4
1x1	13x13	88.69	187.19	2.45	5

Table 9: S/N Comparison FWHM-4 Offset 0

S/N 100					
Start	**Stop**	**Signal**	**StanDev**	**Score**	**Rank**
9x9	11x11	99.88	17.53	0.18	1
9x9	17x17	99.28	18.28	0.21	2
9x9	13x13	97.86	15.56	0.22	3
11x11	13x13	99.73	21.81	0.23	4
9x9	15x15	98.50	18.63	0.23	5
S/N 75					
Start	**Stop**	**Signal**	**StanDev**	**Score**	**Rank**
9x9	21x21	101.20	26.18	0.29	1
9x9	19x19	98.50	24.87	0.30	2
9x9	17x17	102.04	25.21	0.31	3
9x9	15x15	96.96	22.40	0.32	4
9x9	13x13	96.58	22.58	0.34	5
S/N 50					
Start	**Stop**	**Signal**	**StanDev**	**Score**	**Rank**
7x7	17x17	99.62	28.21	0.29	1
7x7	19x19	99.82	30.28	0.31	2
7x7	21x21	98.92	30.98	0.35	3
9x9	15x15	101.98	30.75	0.36	4
9x9	17x17	101.44	33.18	0.37	5
S/N 25					
Start	**Stop**	**Signal**	**StanDev**	**Score**	**Rank**
7x7	21x21	99.55	57.10	0.59	1
7x7	9x9	94.08	49.91	0.71	2
7x7	19x19	95.11	59.92	0.78	3
7x7	15x15	91.46	52.75	0.83	4
9x9	11x11	94.34	64.20	0.85	5
S/N 10					
Start	**Stop**	**Signal**	**StanDev**	**Score**	**Rank**
5x5	19x19	99.82	113.54	1.14	1
7x7	11x11	97.45	127.26	1.38	2
5x5	13x13	87.07	87.82	1.40	3
3x3	15x15	81.94	71.75	1.42	4

3x3	19x19	91.08	107.96	1.45	5
S/N 5					
Start	**Stop**	**Signal**	**StanDev**	**Score**	**Rank**
3x3	19x19	96.27	188.44	2.07	1
3x3	17x17	84.18	148.78	2.24	2
3x3	13x13	73.40	121.82	2.46	3
3x3	21x21	124.22	220.16	2.50	4
5x5	11x11	84.40	179.21	2.59	5
S/N 2					
Start	**Stop**	**Signal**	**StanDev**	**Score**	**Rank**
5x5	9x9	98.96	293.45	3.00	1
5x5	11x11	96.87	329.89	3.50	2
1x1	19x19	104.83	374.88	3.72	3
5x5	13x13	95.13	414.12	4.50	4
3x3	21x21	106.58	473.47	4.64	5

Table 10 is the result of applying the presented algorithm to 60 data sets.

Table 10: Algorithm Application Results

Identifier	S/N	FWHM	Offset	Start	Stop	Signal	StanDev	Score	Rank
1	100	1.5	0	5x5	11x11	99.72	6.71	0.08	1
2	100	2	0	5x5	11x11	99.01	7.33	0.10	2
3	100	2.5	0	7x7	13x13	99.31	13.03	0.15	6
4	100	3	0	7x7	13x13	98.54	11.48	0.16	1
5	100	4	0	9x9	15x15	97.86	15.56	0.22	3
6	100	5	0	11x11	17x17	94.19	23.05	0.42	12
7	100	1.5	0.2	5x5	11x11	99.78	8.01	0.09	2
8	100	2	0.2	5x5	11x11	99.47	8.01	0.10	3
9	100	2.5	0.2	7x7	13x13	99.56	13.08	0.14	2
10	100	1.5	0.4	5x5	11x11	99.43	6.83	0.09	1
11	100	2	0.4	5x5	11x11	99.26	7.87	0.10	1
12	100	2.5	0.4	7x7	13x13	101.03	11.19	0.14	3
13	75	1.5	0	5x5	11x11	99.46	10.46	0.12	2
14	75	2	0	5x5	11x11	99.12	8.36	0.11	1
15	75	2.5	0	7x7	13x13	99.86	13.43	0.14	1
16	75	3	0	7x7	13x13	98.41	15.14	0.20	3
17	75	4	0	9x9	15x15	96.96	22.40	0.32	4
18	75	5	0	11x11	17x17	98.33	31.85	0.37	4
19	75	1.5	0.2	5x5	11x11	99.53	10.65	0.12	6
20	75	2	0.2	5x5	11x11	99.20	10.48	0.13	2
21	75	2.5	0.2	7x7	13x13	97.97	15.12	0.22	9
22	75	1.5	0.4	5x5	11x11	98.58	9.09	0.13	4
23	75	2	0.4	5x5	11x11	100.00	10.39	0.10	1
24	75	2.5	0.4	7x7	13x13	99.82	16.44	0.17	2
25	50	1.5	0	5x5	11x11	101.69	14.29	0.19	7
26	50	2	0	5x5	11x11	100.16	15.71	0.16	1
27	50	2.5	0	7x7	13x13	98.66	23.08	0.27	5
28	50	3	0	7x7	13x13	98.92	23.03	0.27	3
29	50	4	0	9x9	15x15	101.98	30.75	0.36	4
30	50	5	0	11x11	17x17	95.36	40.15	0.56	4
31	50	1.5	0.2	5x5	11x11	99.57	16.32	0.18	5
32	50	2	0.2	5x5	11x11	98.88	15.45	0.19	4
33	50	2.5	0.2	7x7	13x13	99.68	24.55	0.26	3
34	50	1.5	0.4	5x5	11x11	99.56	15.35	0.17	2
35	50	2	0.4	5x5	11x11	99.55	16.47	0.18	2

36	50	2.5	0.4	7x7	13x13	99.59	21.05	0.22	1
37	25	1.5	0	5x5	11x11	102.96	33.45	0.41	9
38	25	2	0	5x5	11x11	99.33	27.80	0.30	1
39	25	2.5	0	7x7	13x13	99.48	45.98	0.48	6
40	25	3	0	7x7	13x13	98.75	48.29	0.53	4
41	25	4	0	9x9	15x15	110.68	72.29	0.97	16
42	25	5	0	11x11	17x17	91.00	101.91	1.39	14
43	25	1.5	0.2	5x5	11x11	107.71	26.83	0.48	13
44	25	2	0.2	5x5	11x11	93.29	30.36	0.53	12
45	25	2.5	0.2	7x7	13x13	107.38	52.05	0.71	16
46	25	1.5	0.4	5x5	11x11	96.62	29.86	0.41	7
47	25	2	0.4	5x5	11x11	97.32	31.75	0.41	4
48	25	2.5	0.4	7x7	13x13	94.34	46.01	0.66	10
49	10	1.5	0	5x5	11x11	97.27	77.08	0.87	10
50	10	2	0	5x5	11x11	92.50	79.85	1.09	8
51	10	2.5	0	7x7	13x13	98.07	135.09	1.44	13
52	10	3	0	7x7	13x13	98.64	115.35	1.21	4
53	10	4	0	9x9	15x15	88.11	176.67	2.36	18
54	10	5	0	11x11	17x17	84.59	238.73	3.28	27
55	10	1.5	0.2	5x5	11x11	96.67	65.71	0.78	5
56	10	2	0.2	5x5	11x11	95.94	71.38	0.87	6
57	10	2.5	0.2	7x7	13x13	100.40	130.01	1.31	12
58	10	1.5	0.4	5x5	11x11	92.00	80.30	1.11	13
59	10	2	0.4	5x5	11x11	98.82	79.37	0.84	5
60	10	2.5	0.4	7x7	13x13	80.54	126.18	2.15	32

Vita

William “Chad” Overcast was born in Tullahoma, TN on June 14, 1983. Chad graduated from Shelbyville Central High in 2001. From there, he went on to the University of Tennessee in Knoxville, TN and received a B.S. in Physics with a minor in Astronomy in 2005. After receiving his degree, Chad went on to work in the Integrated Test & Evaluation department at Arnold Air Force Base. Once there, he continued his education at the University of Tennessee Space Institute in Tullahoma, TN. In May of 2010, Chad received his Master of Science degree in Physics.